35th Annual International Conference of the IEEE EMBS
Osaka, Japan, 3 - 7 July, 2013

Electrical Characteristics of 2D and 3D Microelectrodes for High-Resolution Retinal Prostheses

S. Lee, J. Ahn, H. Yoo, S. Jung, S. Oh, S. Park, and D. Cho*, *Member, IEEE*

***Abstract*— In order to provide high quality visual information to patients who have implanted retinal prosthetic devices, the number of microelectrode should be large. As the number of microelectrode is increased, the dimension of the microelectrode is decreased, which in turn results in the increased interface impedance of microelectrode and decreased dynamic range of injection current. In addition, the reduced maximum limit of injection current may not be sufficiently large to stimulate the ganglion cells in a retina. In order to improve the trade-off envelope between number of microelectrode and current injection limit, a 3D microelectrode structure can be used as an alternative. From the advancement of microfabrication technology, the fabrication of highly-accurate 3D structures with small dimensions is possible. This paper presents a first comprehensive electrical characterization of 2D and 3D microelectrodes for high-resolution retinal prostheses. Microelectrodes which differ in shapes and diameters are analyzed. Their interface impedances and charge injection limits are quantitatively analyzed. This research can be used to define requirements for further retinal prosthetic device research.**

I. Introduction

Retinal degenerative diseases such as retinitis pigmentosa (RP) and age-related macular degeneration (ARMD) are diseases that affect photoreceptors of the retina and cause progressive vision loss, which eventually result in a complete blindness in over 15 million people worldwide [1]. Although blindness caused by photoreceptor degeneration presently remains incurable, inner retinal nerve cells still continue to function for many years despite neuronal remodeling [2]. While pharmaceutical treatments and gene therapy may help maintain vision in the early stages of degeneration, survival of the inner nuclear and retinal ganglion layers support the approach to partially restore vision by electrical stimulation of surviving neurons using neural prostheses devices [3, 4]. Figure 1 shows the schematic diagram of the conventional retinal prosthesis system consisting of several parts, such as an external camera to receive visual information, signal processing circuits, stimulus microelectrode arrays (MEAs), and interconnection wires.

S. Lee, J. Ahn, H. Yoo, S. Oh, S. Park are with the Automation and Systems Research Institute (ASRI) / Inter-university Semiconductor Research Center (ISRC), School of Electrical Engineering and Computer Science, Seoul National University, Seoul, Republic of Korea. (e-mail: sangmlee@snu.ac.kr; brise98@snu.ac.kr; yhj@snu.ac.kr; ohsjsungjin@snu.ac.kr; psk0306@snu.ac.kr).

S. Jung is with the Medical IT Convergence Research Center, Korea Electronics Technology Institute, Seongnam, Gyeonggi Province, Republic of Korea. (e-mail: jungsw@keti.re.kr).

*D. Cho is with the Automation and Systems Research Institute (ASRI) / Inter-university Semiconductor Research Center (ISRC), School of Electrical Engineering and Computer Science, Seoul National University, Seoul, Republic of Korea. (phone: +82-2-880-8371; fax: +1-805-980-4308; e-mail: dicho@snu.ac.kr).

In electrical stimulation methods, MEAs are used to replace the functions of degenerated photoreceptors by delivering electrical signals to surviving inner nuclear and ganglion cell layers [5]. In order to achieve facial-recognition and reading, a high-resolution of visual data is required [6]. However, the number of microelectrodes is limited by overall size of MEAs, which is determined by size of an eyeball. Also, increased number of microelectrodes leads to higher electrode impedance due to the reduction of effective surface area of microelectrodes, which limits the amplitude of injection current [7]. In order to resolve above drawbacks, our research group has developed a fabrication method to implement MEAs with high spatial resolution using 3D microelectrodes without compromising the reduction of effective surface area [8]. Several advantages of 3D microelectrodes are described in our previous research papers [8, 9]. However, to guide the design of a retinal prosthesis, it is necessary to precisely evaluate the feasibility of microelectrode by analyzing the electrical properties, such as electrode-electrolyte interface impedance and maximum allowable current injection limit. Previous researches have been focused on various materials to enhance the electrical characteristics of microelectrodes [10, 11]. In this paper, the electrical characteristics of microelectrode with different shapes and different surface areas are presented. From the measurement result of electrode impedance, each electrode is parameterized using a three-element-circuit model [11] to simulate the current injection limit. Also, the current injection experiment is performed using a current stimulator to verify the simulation result.

Figure 1. Schematic of the conventional retinal prosthesis.

II. Methods

A. Fabrication of Microelectrode

In order to evaluate the advantage of 3D microelectrodes over 2D microelectrodes, two kinds of MEAs are fabricated. The first type of MEA consists of 2D circular microelectrodes with electrode diameter of 25 μm, 50 μm and 75 μm. The second type of MEA consists of 3D arrowhead-shaped microelectrodes, which has base electrode diameter of 25 μm,

50 μm and 75 μm. The fabrication of 2D circular microelectrode is performed by simple patterning process of upper and lower polyimide layers, and Au metal patterning process between two polyimide layers [12]. The 3D arrowhead-shaped microelectrode is fabricated by silicon mold fabrication utilized by anisotropic silicon wet etching process, Au electroplating process, and polyimide patterning process [8]. The fabricated MEAs are shown in Figure 2 (a), (b). Each MEA consists of three arrays with 16 microelectrodes which differ in diameter. The fabricated MEAs are wire-bonded to a printed-circuit board (PCB) to measure electrode-electrolyte interface impedance and the current injection property.

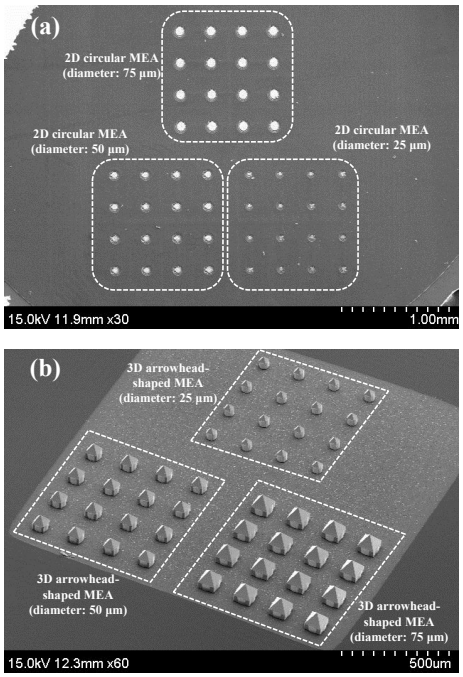

Figure 2. Fabrication and implementation results. (a) 2D circular MEA. (b) 3D arrowhead-shaped MEA.

B. *Experimental Set-Up*

In order to measure the interface impedance, an impedance analyzer, SI 1287 & SI 1260 (Solatron, USA) is used. The experimental set-up is shown in Figure 3 (a). In order to measure the current injection limit of each microelectrode, a current stimulator [13] developed in our research group is used. The schematic diagram of the implemented current stimulator is shown in Figure 3 (b). The circuit uses two microelectrodes, which one is for sourcing stimulation current and the other is for sinking stimulation current. As shown in the circuit diagram, the circuit contains a sensor to measure the injection current.

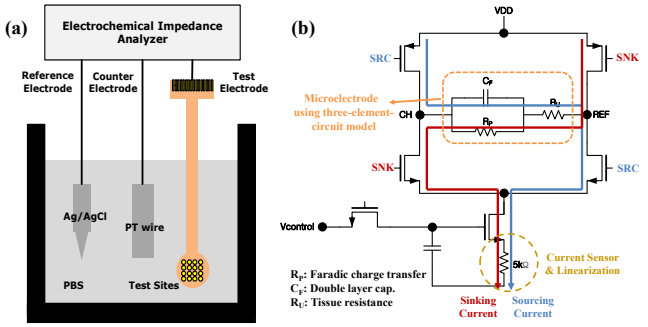

Figure 3. Experimental set-up. (a) Impedance measurment. (b) Schematic of current stimulator.

III. RESULTS

A. *Electrode Impedance*

The measurement results of interface impedance are shown in Figure 4 and summarized in TABLE I. The impedance is measured at 1 kHz, since the conventional current stimulation method is performed using biphasic current of 1 ms pulse duration. As the effective surface area increases, the impedance at frequency of 1 kHz is decreased. As a consequence, 3D arrowhead-shaped microelectrode which has the base diameter size of 25 μm results in similar interface impedance value as 2D circular microelectrode with base diameter of 75 μm.

TABLE I. SUMMARIZED RESULT OF INTERFACE IMPEDANCE MEASUREMENT

@ 1 kHz	**2D circular electrode**			**3D arrowhead-shaped electrode**		
Diameter (μm)	25	50	75	25	50	75
Base area (μm^2)	491	1,963	4,418	491	1,963	4,418
Surface area (μm^2)	491	1,963	4,418	4,802	11.354	19,656
Surface area/base area	1	1	1	~ 10	~ 6	~ 4
Area ratio compared to 2D 25 μm	1	~ 4	~ 9	~ 10	~ 23	~ 40
Conversion to 2D circular electrode	25	50	75	~ 78	~ 120	~ 158
Impedance (kΩ)	2,850	817	248	212	29.0	7.19
Impedance ratio compared to 2D 25 μm	1	0.29	0.087	0.074	0.0098	0.0025
Image	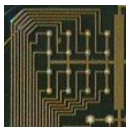	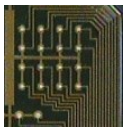	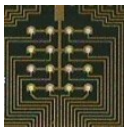	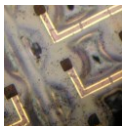	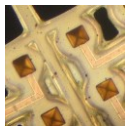	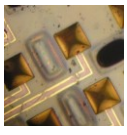

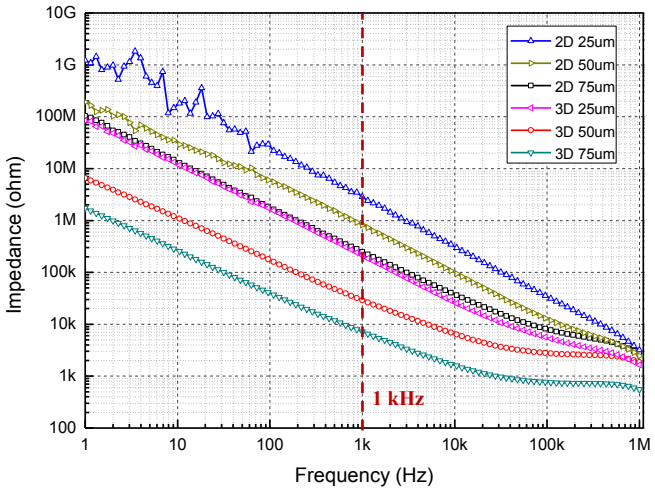

Figure 4. Electrode-electrolyte interface impedance measurement result.

B. Circuit Modeling Using SPICE

In order to investigate the characteristics of each microelectrode, the measured impedance results are parameterized using a three-element-circuit model, where R_P, C_F and R_U are faradic charge transfer, double layer capacitance and tissue resistance, respectively. The schematic of the simulation model is in Figure 5 and the estimated value is summarized in TABLE II. Each parameter is determined from the measurement results of interface impedance in order of magnitude. After applying the model parameters in the three-element circuit model, the model is simulated using a SPICE. The simulation result of interface impedance is shown in Figure 6. The simulated values fit with the measurement results as shown in TABLE III.

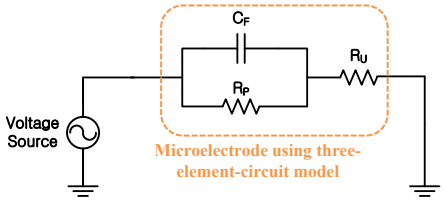

Figure 5. Three-element circuit model.

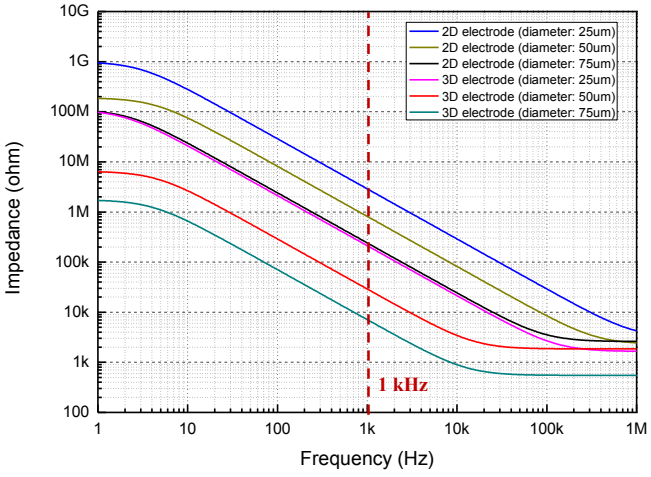

Figure 6. Simulated impedance using SPICE.

TABLE II. SUMMARIZED PARAMETERS

Shape & size	2D circular microelectrode			3D arrowhead-shaped microelectrode		
	25 μm	*50 μm*	*75 μm*	*25 μm*	*50 μm*	*75 μm*
R_P	1 GΩ	190 MΩ	110 MΩ	110 MΩ	6.5 MΩ	1.75 MΩ
C_F	55 pF	195 pF	660 pF	750 pF	5.5 nF	22.5 nF
R_U	3.1 kΩ	2.3 kΩ	2.6 kΩ	1.65 kΩ	1.85 kΩ	0.55 kΩ

TABLE III. SIMULATED IMPEDANCE SUMMARY

@ 1 kHz	2D circular microelectrode			3D arrowhead-shaped microelectrode		
	25 μm	*50 μm*	*75 μm*	*25 μm*	*50 μm*	*75 μm*
Impe-dance	2.89 MΩ	816 kΩ	241 kΩ	212 kΩ	29 kΩ	7.1 kΩ
Error	1.4 %	0.12 %	2.8 %	0.02 %	0.15 %	1.3 %

C. Injection Current Limit Simulation

After deriving the circuit model parameters, each model is simulated by an AC voltage source with magnitude of 1 V. The simulation result is shown in Figure 7 and summarized in TABLE IV. The results indicate that the maximum amplitude of current is limited at specific frequency. Also, as the effective surface area of microelectrode is increased, the maximum allowable injection current is increased. Another meaningful result is that as current stimulation is performed under higher frequency than 1 kHz (or 1 ms pulse duration), the allowable current limit is exceeded.

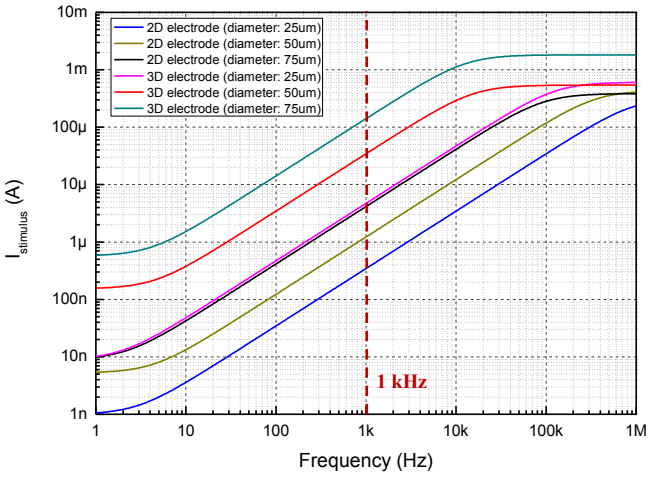

Figure 7. Simulated stimulation current using SPICE.

TABLE IV. SIMULATED STIMULATION CURRENT SUMMARY

@ 1 kHz	2D circular microelectrode			3D arrowhead-shaped microelectrode		
	25 μm	*50 μm*	*75 μm*	*25 μm*	*50 μm*	*75 μm*
$I_{STIMULUS}$	0.34 μA	1.23 μA	4.15 μA	4.71 μA	34.5 μA	141 μA

D. Maximum Allowable Current Injection Limit

In order to evaluate the maximum allowable current injection limit, each MEA is tested using the current stimulator. Each fabricated MEA are dipped in a phosphate buffered saline (PBS) solution. The maximum current that the stimulator can generate is 512 μA, which is large enough to stimulate the ganglion cells in retina. The experiment is performed under various pulse durations. The result is shown in Figure 8 and summarized in TABLE V. The maximum current injection limit of 3D arrowhead-shaped microelectrode is extremely higher compared to that of 2D circular microelectrode due to the enlargement of effective surface area.

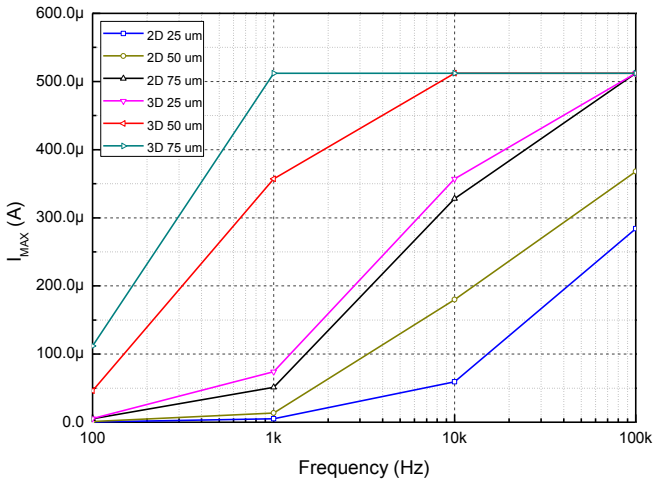

Figure 8. Experimental result of maximum allowable current.

TABLE V. SUMMARIZED RESULT OF MAXIMUM ALLOWABLE CURRENT

Type	Pulse duration (operation voltage @ 12V)		
	Measured 1 ms (1 kHz)	*Simulated 1 ms (1 kHz)*	*Error*
25 μm (2D)	5.12 μA	4.08 μA	20.3 %
50 μm (2D)	13.6 μA	14.8 μA	8.53 %
75 μm (2D)	51.2μA	49.8 μA	2.73 %
25 μm (3D)	74 μA	56.5 μA	23.6 %
50 μm (3D)	257 μA	414 μA	15.9 %
75 μm (3D)	512 μA (max)	1,692 μA	Not available

IV. CONCLUSIONS

This paper presents electrical characterization of 2D and 3D microelectrode for high-resolution retinal prostheses. For sufficient stimulation of the ganglion cells of the retina, a large dynamic range of injection current is necessary. Conventional methods have chosen to enlarge the diameter of the microelectrode to deliver a large dynamic range of injection current. However, for high-resolution retinal prostheses, the trade-off between number of microelectrode and current injection limit is a major constraint, because the limit is mainly influenced by the effective surface area of the microelectrode. Therefore, a 3D microelectrode structure can be used as an alternative, which is able to improve the trade-off envelope. The maximum current injection limit of 2D circular microelectrode with diameter of 75 μm and 3D arrowhead-shaped microelectrode with diameter of 25 μm show similar result. This implies that MEA with 3D arrowhead-shaped microelectrodes is able to achieve 9 times higher spatial resolution than MEA with 2D circular microelectrodes in the same substrate region. From the result, to implement over 1,000 microelectrodes in the MEA which has the size of 3 mm × 3mm, the 3D microelectrodes is preferred considering the spacing between microelectrodes. In addition, this research can be used to define requirements for further high-resolution retinal prosthetic device research.

ACKNOWLEDGMENT

This research was supported by the public welfare & safety research program through the National Research Foundation of Korea (NRF) funded by the Ministry of Education, Science and Technology (2012-0008611).

REFERENCES

[1] N. Congdon, B. O'Colmain , C. C. Klaver, R. Klein, B. Munoz, D. S. Friedman, J. Kempen , H. R. Taylor, P. Mitchell, "Causes and prevalence of visual impairment among adults in the United States," *Arch. Ophthalmol.*, vol. 122, pp. 477-485, 2004.

[2] B. W. Jones, R. E. Marc, "Retinal remodeling during retinal degeneration," *Exp. Eye Res.*, vol. 81, pp. 123-137, 2005.

[3] E. Zrenner, A. Stett, S. Weiss, R. B. Aramant, E. Guenther, K. Kohler, K. D. Miliczek, M. J. Seiler, H. Haemmerle, "Can subretinal microphotodiodes successfully replace degenerated photoreceptors?," *Vis. Res.*, vol. 39 pp. 2555-2567, 1999.

[4] M. Humayun, R. Propst, E. de Juan Jr., K. McCormick, D. Hickingbotham, "Bipolar surface electrical stimulation of the vertebrate retina," *Arch. Ophthalmol.*, vol. 112, no. 1, pp.110-116, 1994.

[5] E. Zrenner, K. U. Bartz-Schmidt, H. Benav, D. Besch, A. Bruckmann, V. P. Gabel, F. Gekeler, U. Greppmaier, A. Harscher, and S. Kibbel, "Subretinal electronic chips allow blind patients to read letters and combine them to words," *Proc. R. Soc. B.*, vol. 278, no. 1711, pp. 1489-1497, 2011.

[6] A. P. Fornos, J. Sommerhalder, B. Rappaz, A. B. Safran, and M. Pelizzone, "Simulation of artificial vision, III: Do the spatial or temporal characteristics of stimulus pixelization really matter?," *Invest. Ophthalmol. Vis. Sci.*, vol. 46, no. 10, pp. 3906-3912, 2005.

[7] K. Chen, Z. Yang, L. Hoang, J. D. Weiland, M. S. Humayun, and W. Liu, "An integrated 256-channel epiretinal prosthesis," *IEEE J. Solid-State Circuits*, vol. 45, no. 9, pp. 1945-1956, 2010.

[8] K. Koo, S. Lee, S. H. Bae, J. M. Seo, H. Chung, and D. Cho, "Arrowheadshaped microelectrodes fabricated on a flexible substrate for enhancing the spherical conformity of retinal prostheses," *J. Microelectromech. Syst.*, vol. 20, no. 1, pp. 251-259, 2011.

[9] S. Hong, S. Lee, H. Yoo, J. Ahn, S. Park, K. Koo, and D. Cho, "Mechanical and electrical evaluation for the long-term stability of implanted 3D retinal microelectrode," *Solid-State Sensors, Actuators and Microsystems Conference (TRANSDUCERS), 2011 16th International* , vol. 1, no. 1, pp. 202-205, 5-9 June 2011.

[10] O. Niina, T. Hirotaka, K. Yoshiuki, K. Toshiya, K. Risato, T. Tetsu, and H. Jari, "Comparison of electrode materials for the use of retinal prosthesis," Biomed. Mater. Eng., vol. 21, no. 2, pp. 83-97, 2011.

[11] S. Shah, A. Hines, D. Zhou, R. J. Greenberg, M. S. Humayun, and J. D. Weiland, "Electrical properties of retinal–electrode interface," *J. Neural Eng.*, vol. 4, no. 1, pp. S24, 2007.

[12] K. Koo, S. Lee, J. H. Yee, S. B. Ryu, K. H. Kim, Y. S. Goo, and D. Cho, "A novel *in-vitro* sensing configuration for retinal physiology analysis of a sub-retinal prosthesis," *Sensors*, vol. 12, no. 3, pp. 3131-3144, 2012.

[13] J. H. Ahn, S. Lee, S. J. Hong, H. J. Yoo, S. W. Jung, S. K. Park, H. H. Ko, and D. Cho, "Multi-channel stimulator IC using a channel sharing method for retinal prostheses," *J. biomed. Nanotechnol.*, vol. 9, pp. 621-625, 2013.